Asian Pub. Corp.

www.asianpubs.org

ARTICLE

Docking and Molecular Dynamic Simulation of Temozolomide with Carbonic Anhydrase XIII

R. Meenashi[1], K. Selvaraju[1,✉], P. Jayalakshmi[1], P.V. Nidhin[2] and A. David Stephen[3]

ABSTRACT

The effect of inhibition of temozolomide, an alkylating agent widely used in cancer treatments, with carbonic anhydrase XIII protein was investigated using docking studies. The stability of temozolomide in the protein environment was assessed and analyzed by molecular dynamics simulation. The topological and charge density variations of temozolomide were studied in detail to perceive the primary insight of the pharmaceutical actions.

KEYWORDS

Temozolomide, Docking, Carbonic anhydrase XIII, Binding energy.

Asian Journal of Organic & Medicinal Chemistry

Volume: 5 Year: 2020
Issue: 4 Month: October–December
pp: 332–339
DOI: https://doi.org/10.14233/ajomc.2020.AJOMC-P300

Received: 27 November 2020
Accepted: 19 December 2020
Published: 31 December 2020

Author affiliations:

[1]Department of Physics, Kandaswami Kandar's College, Velur-638182, India
[2]Department of Physics, Safa College of Arts and Science, Valanchery-676552, India
[3]Department of Physics, PSG College of Arts and Science, Coimbatore-641014, India

✉To whom correspondence to be addressed:

E-mail: physicsselvaraj@gmail.com

Available online at: http://ajomc.asianpubs.org

INTRODUCTION

Glioblastoma is considered as an aggressive primary brain tumor when compared with the other malignancies of the brain which occur less frequently (2% occurrence of all human cancers) [1]. Despite the advanced surgical treatment, these tumors are subject to frequent reoccurrences with serious consequences. In most cases, the survival time of glioblastoma patients remains shorter than a year even after treatment with advanced radiotherapy. It was reported that the patients with anaplastic gliomas have longer survival periods extended up to 5 years but with severe side effects includes seizures and progressive neurological disability [2]. Researchers have undergone their efforts with various chemotherapeutic drugs to improve the survival time for many decades. It was strongly believed that the blood-brain barrier was the primary hindrance in treating glioblastoma with chemotherapies and thus the drugs that were capable of crossing this barrier were selected preferentially [3].

Temozolomide, a potential DNA methylating chemotherapeutic drug, is used to prevent the growth of this aggressive brain tumor and readily crosses the blood-brain barrier [4]. The biological activity of temozolomide is established by the inhibition of carbonic anhydrases [5]. The intracellular pH of malignant gliomas is alkaline, compared to the normal brain, whereas the extracellular compartment is highly acidic. Carbonic anhydrases catalyze the inter conversion between CO_2 and bicarbonate with the release of a proton and are involved in pH regulation and metabolism. At least 15 CA isoforms are present in humans, 12 of which are catalytically active and drug targets (CA I-IV, CA VI-VII, CA IX, CA XII-XIV, CA VA, CA VB). Of the 15 carbonic anhydrase isoforms expressed

in humans, only CA IX and CA XII have been implicated in cancer [6]. These enzymes are *trans*-membrane proteins in which their extracellular domain contains the catalytic activity, positioning them in the regulation of tumor microenvironment. The role of carbonic anhydrase XIII (CAXIII) in the chemo-resistance of glioblastoma is unexplored.

In present study, we identified that the temozolomide is a potential inhibitor of CA XIII from the molecular docking, charge density analysis and the molecular dynamic simulation. In drug design, the nature of the interaction between ligand and protein, binding affinity, stability of ligand in the active site of CA XIII are the essential parameters; therefore, the molecular conformation, charge density distribution and the electrostatic properties of ligand molecules were computed. Furthermore, molecular dynamic simulation has been performed for this CA XIII-temozolomide complex to understand the stability of the molecule in the active site of the enzyme. The present study gives the conformational behaviour, intermolecular interactions, stability and the binding free energy of temozolomide–CA XIII complex.

COMPUTATIONAL DETAIL

Molecular docking: The crystal structure of the human carbonic anhydrase isozyme XIII enzymes was retrieved from the RCSB (PDB: 6G5U) [7] and prepared for the molecular docking after removal of the chain B, water molecules (beyond 4 Å) and adding hydrogen, charges, formal bond orders. Further, the molecular docking studies have been performed by using Schrodinger 2018 software [8]. Intermolecular interactions such as hydrogen bonding, hydrophobic interactions were analyzed with the help of PyMol [9]. The best conformer was taken to perform the molecular dynamics based on score and intermolecular interactions.

Molecular dynamics and binding free energy calculation: The initial coordinates from molecular docking were used to create the topology files for the molecular dynamic simulations using antechamber (ligand molecule) and leap (complex) modules with the Gaff and AMBER ff14SB [10] force fields using AMBERTOOLS14 package [11]. The complex system was immersed in a water box with an orthorhombic shell of TIP3P at 9 Å distance of a minimum solute-wall [12] after neutralizing the system by adding counter-ions (Na^+). Further, the system was minimized using steepest descent and conjugate gradient methods to remove the steric clashes and annealing was processed from 0 to 300 K using canonical ensemble (NVT) [13]. The complex was subjected to production phase and extended up to 10 ns in 2 fs time step at constant temperature (300 K) and pressure (1 bar) using isothermal-isobaric ensemble (NPT) [14]. The SHAKE algorithm is used to constrain the non-polar hydrogen atoms. The molecular dynamic trajectories were taken to analyze the root mean square deviations (RMSD), the root mean square fluctuations (RMSF), the radius of gyration (R_g) and intermolecular interactions with the help of VMD and CPPTRAJ software [15-17]. Further, the MM/GBSA of the CA XIII-TMZ complex was calculated using the following equations:

$$\Delta G_{bind} = \Delta G_{complex} - \{\Delta G_{receptor} + \Delta G_{ligand}\} \quad (1)$$

This all terms were easy way to calculate from MMPBSA.py implemented in AMBERTOOLS14 package [18,19] by using 1000 frames (MD trajectories) and the LCPO algorithm.

QTAIM analysis: To understand the molecular geometry, topological and electrostatic properties of temozolomide along with active site residues, a single point energy DFT calculation was performed at B3LYP/6-311G level [20] using Gaussian03 software [21]. The Bader's quantum theory of atoms in molecules (AIM) was used to determine the electron density at the bond critical point (bcp) of the molecule using AIMPAC software [22] and mapped by using wfn2plot and denprop available in XD2006 software [23]. The hydrogen bonding interaction of temozolomide with active site residues has been investigated and the corresponding bond topological characteristics were analyzed using QTAIM approach. The electrostatic potential (ESP) map of the molecule has been generated from the 3Dplot in WinXPRO software [24] package.

RESULTS AND DISCUSSION

Interaction of temozolomide with target protein: The interaction of temozolomide drug towards CA XIII was analyzed from the molecular docking. Fig. 1 represents the orientation of temozolomide molecule towards the binding site of the CA XIII.

Table-1 lists the different docking scores of the ten best poses of the ligand in the CA XIII binding site. In which, the best pose exhibits the lowest docking score and IFD score, the values are –5.27 and –524.19 kcal/mol, respectively. It was observed that the expected active site amino acids were involved in the interactions with ligand. Amongst, the residues THR201, GLN94, SER199 and HIS121 were considered active participants in the binding region which forms the strong interactions with temozolomide molecule.

TABLE-1
DIFFERENT BINDING SCORE AND ENERGY (kcal/mol) VALUES OF THE 10 BEST POSES

S. No.	Docking score	Glide model	Glide energy	IFD score
1	-5.27	-46.50	-34.17	-524.19
2	-5.48	-50.12	-36.47	-524.10
3	-5.52	-50.50	-37.26	-523.95
4	-4.62	-46.83	-34.38	-523.39
5	-4.93	-45.37	-33.85	-523.34
6	-4.62	-40.46	-31.61	-522.93
7	-3.88	-41.52	-36.43	-522.24
8	-3.86	-31.43	-25.68	-522.05
9	-3.80	-41.40	-31.25	-522.04
10	-2.82	-38.16	-30.71	-521.25

The possible interactions of TMZ with amino acids of CA XIII are listed in Table-2. A strong hydrogen bond interaction was framed from formaldehyde and acetamide groups of temozolomide. In docking, four strong H-bond interactions were noticed; the oxygen atom of formaldehyde group with GLN94; oxygen atom of acetamide with THR201 and HIS121 residues and the nitrogen atom of acetamide with SER199, respectively. Among the H-bond interactions, the oxygen atoms [O1/O2] of the ligand which makes their H-bond with THR201, GLN94 and HIS121 was considered as the strongest with the

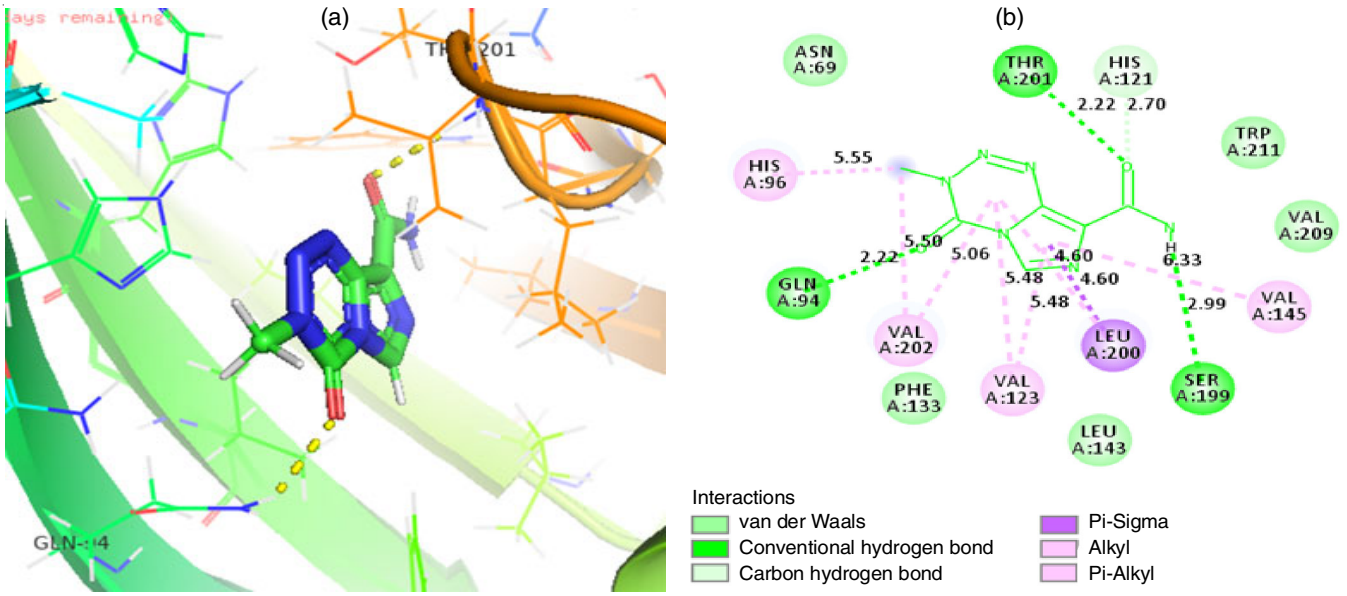

Fig. 1. View of the intermolecular interactions in the docked complex (a) 3D and (b) 2D plot

interacting distances 2.22, 2.22 and 2.70 Å, respectively. The stabilization of the ligand molecule in the active site was further established from other weak interactions such as π-σ, π-alkyl and alkyl interactions (Table-2).

Topological properties of ligands and interactions with protein: The topological analysis of electron density was carried out for temozolomide molecule with the neighboring interacting amino acids (within contact distance around 4 Å) in the active site of CA XIII. The critical point (cp) search has been carried out for all interactions and found a (3, –1) type of cp for these interactions. Further, the deformation electron density maps are also plotted, which reveals the charge accumulation in the bonding region, lone pair positions of atoms in the molecule. The Laplacian of electron density map displays the charge concentration and the charge depletion at the cp's of chemical bonds. Further, the topological properties of strong intermolecular interactions are also calculated to understand the electron density at, cp which helps to characterize the intermolecular interactions.

TABLE-2
HYDROGEN BONDING DETAILS OF THE INTERACTIONS OF DOCKED MOLECULE TMZ WITH TARGET CA XIII PROTEIN

Interactions	Distance	Type
O2....HN/THR201	2.22	H-bond
O1....HN/GLN94	2.22	
O2....HC/HIS121	2.70	
N6-H6....O/SER199	2.99	
Imidazole....HC/LEU200	2.80	π-σ
Imidazole....VAL123	4.18	π-Alkyl
Imidazole....VAL145	4.99	
Tetrazine....VAL123	4.92	
Tetrazine....VAL202	4.47	
Tetrazine....LEU200	5.07	
C5....HIS96	4.47	
C5....VAL202	4.86	Alkyl

The electron density and Laplacian of the electron density mappings of the molecule show the covalent bonding regions and lone pairs of the oxygen atoms that are shown in Figs. 2 and 3. The topological properties of the electron density of

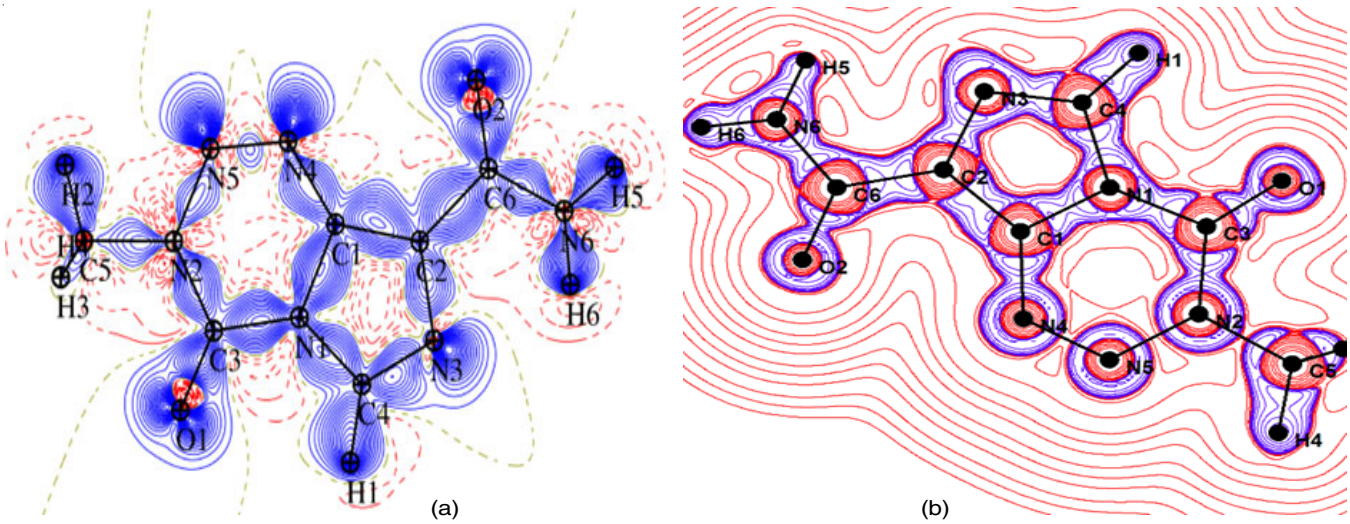

Fig. 2. Deformation (a) and Laplacian electron density (b) map of covalent bonds of TMZ molecule in the active site of CA XIII. The blue colour represents positive contours (solid lines), the red colour represents negative contours (dotted lines)

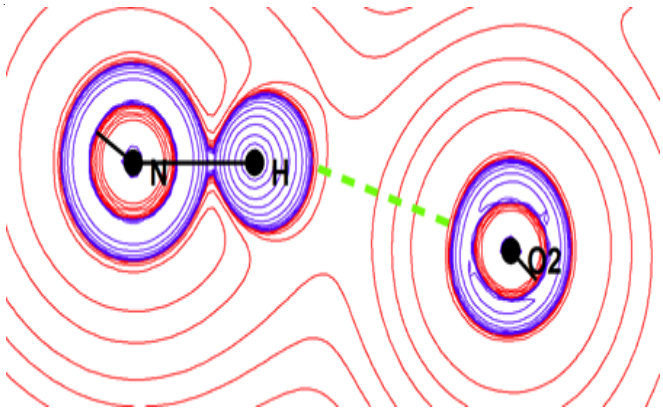

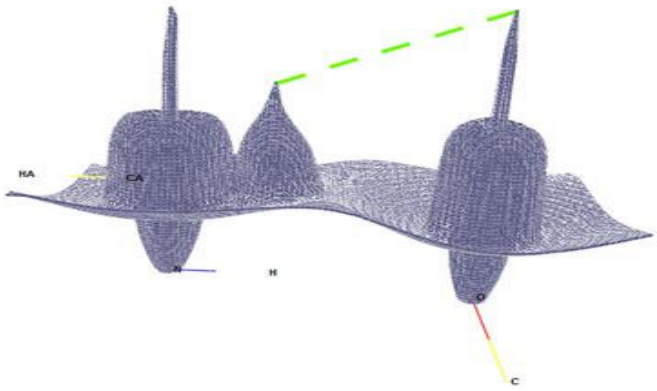

(a) O2….HN/THR201

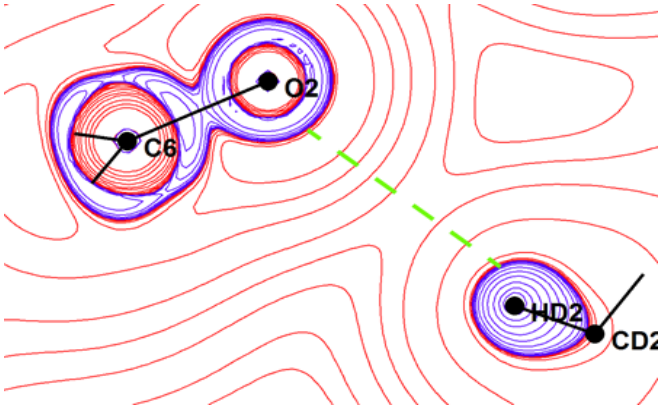

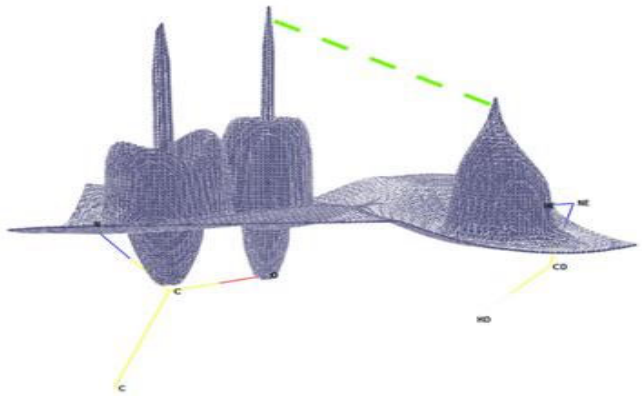

(b) O2…HC/HIS121

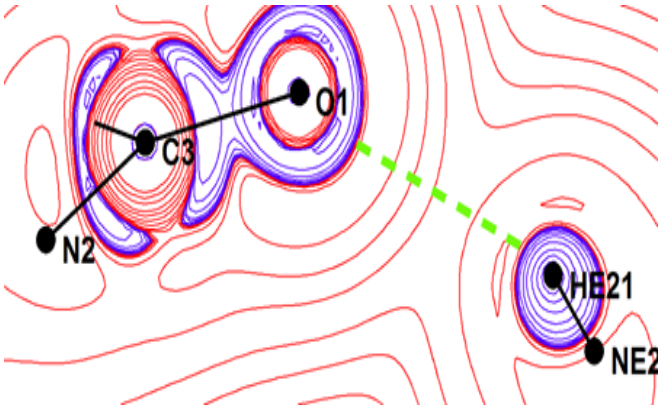

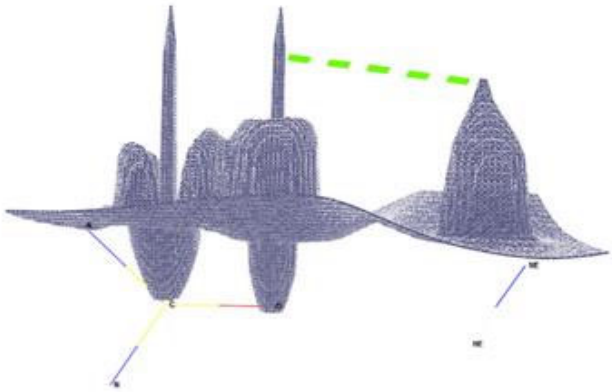

(c) O1….HN/GLN94

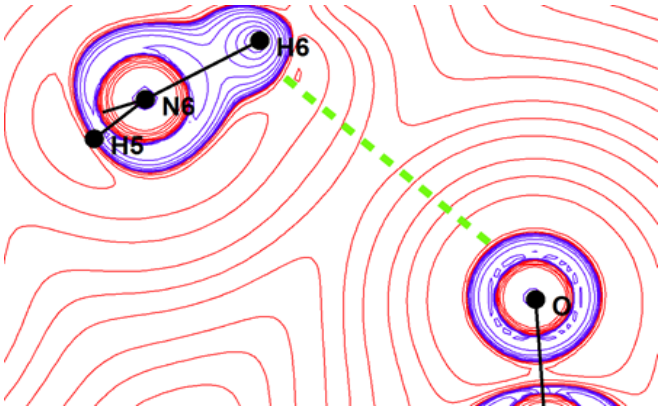

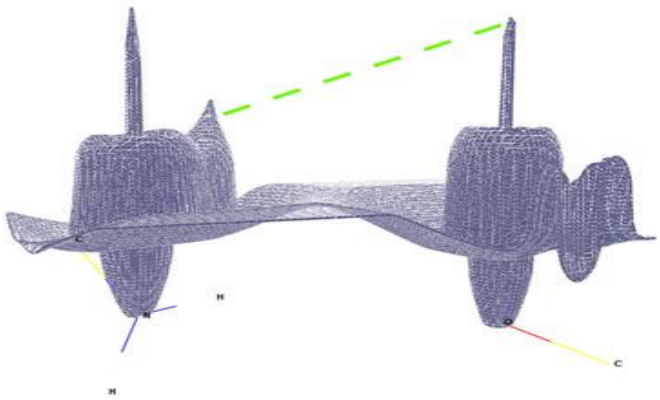

(d) N6H6…O/SER199

Fig. 3. Laplacian of electron density map of intermolecular interactions of TMZ and CA XIII enzyme obtained from DFT calculation in contour and relief mode (range: -250 to +250 eÅ^{-5}) [a-d]. Contours are drawn in logarithmic scale, 3.0 2^{N} eÅ^{-5}, where, N = 2, 4 and 8 × 10^{n}, n = –2, –1, 0, 1, 2. Blue (solid lines): positive contour and red (dashed lines): negative contour

the molecule both in the gas phase and in active site are listed in Table-3.

TABLE-3
TOPOLOGICAL PROPERTIES OF ELECTRON DENSITY OF TMZ IN THE GAS PHASE (B3LYP/6-311G) AND IN THE ACTIVE SITE OF CA XIII

Bonds	$\rho_{bcp}(r)$		$\nabla^2\rho_{bcp}(r)$	
	Gas	Active site	Gas	Active site
C(2)-C(1)	2.152	2.104	-21.064	-20.194
C(1)-N(1)	1.993	2.109	-18.158	-16.648
N(3)-C(4)	2.472	2.496	-26.933	-26.049
C(2)-N(3)	2.181	2.351	-24.715	-23.482
N(1)-C(4)	2.083	2.066	-15.265	-15.552
N(2)-C(3)	2.144	2.204	-25.449	-26.638
N(1)-C(3)	2.034	1.956	-23.72	-22.121
N(4)-C(1)	2.236	2.244	-27.383	-27.334
N(5)-N(2)	2.235	2.275	-12.98	-13.56
N(4)-N(5)	3.018	2.717	-24.137	-18.997
C(6)-C(2)	1.825	1.997	-16.742	-20.062
N(6)-C(6)	2.19	2.306	-24.501	-22.88
O(2)-C(6)	2.745	2.736	-0.535	-1.965
C(3)-O(1)	2.813	2.716	-0.536	-3.799
N(2)-C(5)	1.727	1.699	-16.293	-15.686
H(6)-N(12)	2.32	2.31	-44.119	-44.264
C(4)-H(1)	1.988	1.987	-27.727	-27.57
H(2)-C(5)	1.921	1.923	-24.755	-24.772
C(5)-H(3)	1.921	1.926	-24.749	-25.004
H(4)-C(5)	1.943	1.922	-25.595	-25.06
N(12)-H(5)	2.314	2.329	-44.222	-44.512

Among the C-N bonds in the imidazole ring, C4-N3 bond in both gas phase and active site exhibits high electron density at the bcp and the values are 2.47 and 2.50, respectively. This characteristics of this bond were well established from the high negative Laplacian values, -26.9 and -26.0, which shows that the charges are highly concentrated in its binding region.

The average electron density at the bcp of C-N bonds in the imidazole ring is ~2.13 calculated for both gas and active site environment. The QTAIM analysis of homogenous N-N bonds [N2-N5 and N5-N4] reveals that electrons are highly localized in the bonding region of N5-N4 bond, where the electron density and Laplacian values are 3.02 and -24.1 in the gas phase. The respective values were feebly reduced [2.72 and -19.0] in the active site environment, as the N5-N4 bond is slightly stretched by 0.5 in protein surrounding. There is no significant difference was found for N2-N5 bonds, as their ρ and del2rho values were 2.23/2.27 and -13/-13.1, respectively. As expected, the value of ρ at the bcp of C=O bonds in formaldehyde and acetamide groups is high among all other bonds of TMZ, both in gas and active site and the average values are 2.78 and 2.73 Å, respectively. On contrary, the negative sense of the corresponding Laplacian values is very low, as their average values are -0.53 and -2.88, respectively. This discrepancy is due to the different behaviour of Gaussian and Slater-type radial functions at the vicinity of the bcp and a similar trend were studied in the various report [25-27].

The bond critical point search on these interactions produced a (3, –1) type of critical points between atoms in temozolomide and the neighboring amino acid of temozolomide-CA XIII complex. The H-bond topological parameters are listed in Table-4. The positive value of the Laplacian confirms that these interactions are a closed-shell type of interaction. Fig. 4

TABLE-4
TOPOLOGICAL PROPERTIES OF INTERMOLECULAR INTERACTIONS

Bond	ρ_{bcp} (r)	$\nabla^2\rho_{bcp}$ (r)	ε	V(r)	G(r)	H(r)	d1	d2	D
O2....HN/THR201	0.10	1.02	0.05	-0.07	0.07	0.00	1.358	0.892	2.250
O1....HN/GLN94	0.10	1.42	0.44	-0.08	0.09	0.01	1.318	1.003	2.321
O2....HC/HIS121	0.04	0.52	0.19	-0.02	0.03	0.01	1.579	1.161	2.741
N6....O/SER199	0.02	0.35	0.42	-0.02	0.02	0.00	1.797	1.660	3.457

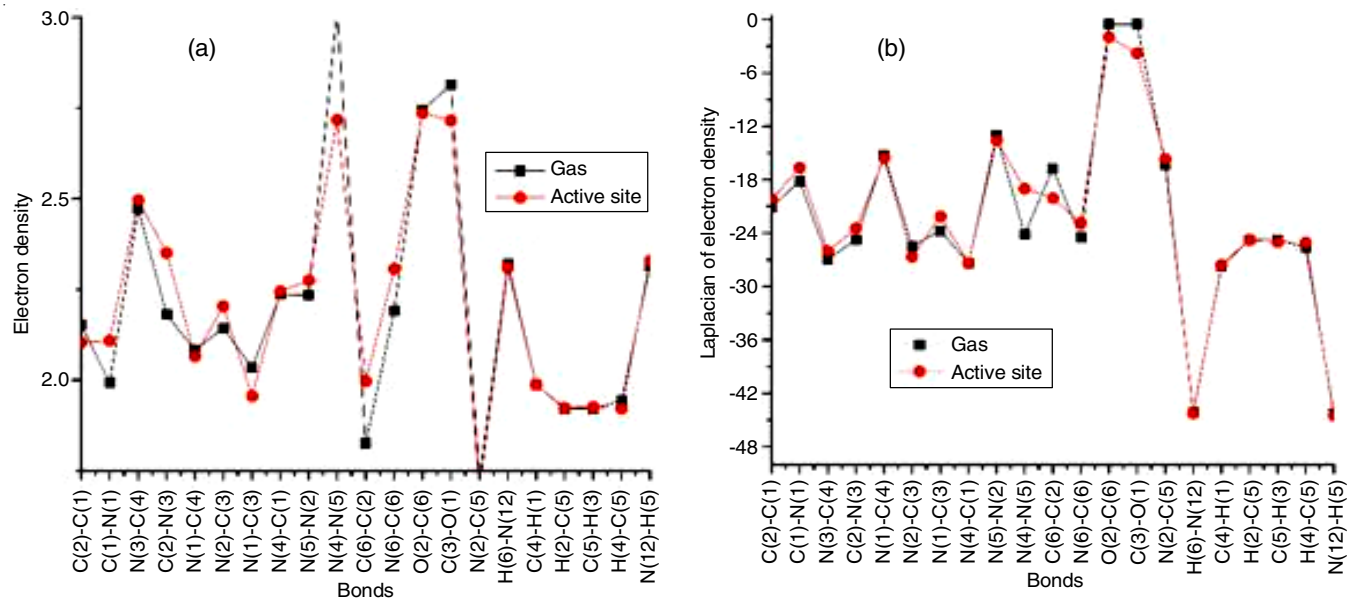

Fig. 4. Difference of (a) electron density $\rho_{bcp}(r)$ and (b) the Lapalacian of electron density $\nabla^2\rho_{bcp}(r)$ of TMZ molecule in the gas phase and in the active site of CA XIII

shows the relief plot of Laplacian of electron density of hydrogen bonding interactions. On the whole slight variations were observed in the topological characteristics of temozolomide in the gas phase and active site for N4-N5, C6-C2 and C=O bonds. This difference established the interaction of temozolomide ligand with amino acids of CA XIII.

The relief illustrates the alignment of lone pairs of O atoms involved in the intermolecular interaction. The contacts O2….HN/THR201 and O1….HN/GLN94 has the highest electron density value, 0.10 e/Å^3 which shows the strength of the contact.

Electrostatic potential: The electrostatic potential of the temozolomide molecule both in the gas phase and the active site environment is shown in Fig. 5. As observed there is a negative potential in the vicinity of oxygen atoms [O1 and O2] of both formaldehyde and acetamide groups of temozolomide in the active site of CA XIII environment, whereas in gas phase temozolomide, the negative potential is found only for formaldehyde oxygen atom [O1]. It was concluded that there are strong hydrogen bond interactions between the oxygen atoms, O1 and O2 with GLN94, THR201 and HIS121 amino acid residues of CA XIII. The negative isosurface value of -0.05e/Å is used to draw the negative surface (red) of temozolomide exhibited both in the gas phase and active site.

Conformational stability and free energy calculation: The docking tool helps to determine the binding affinity of the drug-receptor complex; whereas, molecular dynamic is used to understand the movement of the complex concerning time and to assess the stability of the docked pose. In this work, a new inhibitor against CA-XIII is approached, which exhibits a potential activity as well as take over the full binding cavity of the CA-XIII.

The root mean square deviation (RMSD) is the important property to determine the atomic position of the protein-ligand complex concerning initial coordinates. The average RMSD of temozolomide-CA-XIII complex is ~2 Å. The radius of gyration (Rg) is used to examine the compactness of the protein. The Rg of the complex shows that the complex has stable compactness (~18 Å). The root mean square fluctuation (RMSF) is another important property to evaluate the backbone fluctuation. In general, the loop regions are more fluctuating than the secondary structures due to the deviation of intramolecular interactions. Particularly, lesser fluctuations are noticed in the active site regions (Fig. 6); this is strongly attributed due to the effect of intermolecular interactions. To estimate the binding energy of temozolomide-CA-XIII complex, the enthalpy was calculated. The total enthalpy based binding energy is -17.96 kcal/mol; calculated from the H-bond, electrostatic and van der Waals interactions. This high polar value is attributed to the fact that the ligand molecule contains highly polar groups (Table-5).

TABLE-5
CONTRIBUTIONS OF VARIOUS ENERGY COMPONENTS TO THE BINDING FREE ENERGY (kcal/mol) FOR THE TEMO-HUMAN CARBONIC ANHYDRASE ISOZYME XIII ENZYME COMPLEX

Binding energy	MM/GBSA
ΔE_{vdw}	-27.6 (1.8)
$\Delta E_{electrostatic}$	-13.4 (3.2)
$\Delta G_{PB/GB}$	26.4 (2.2)
ΔG_{SA}	-3.3 (0.1)
ΔE_{gas} (E_{MM})	-41.1 (3.9)
ΔG_{sol}	23.1 (2.2)
ΔG_{total}	-18.0 (2.6)

Conclusion

Temozolomide drug was successfully docked in the active site of carbonic anhydrase XIII protein using the glide docking. The stability of the docking mechanism was determined by IFD methods which analyzing the binding energy and docking scores exhibiting the residues THR201, GLN94, SER199 and HIS121 as an active participant in the binding region which forms the strong interactions with temozolomide molecule. The stability of the drug molecule in the active site was authenticated from the possible hydrogen bond interactions which prevailed in the binding. The variations in the energy density and the nature of the chemical bonds of temozolomide in active

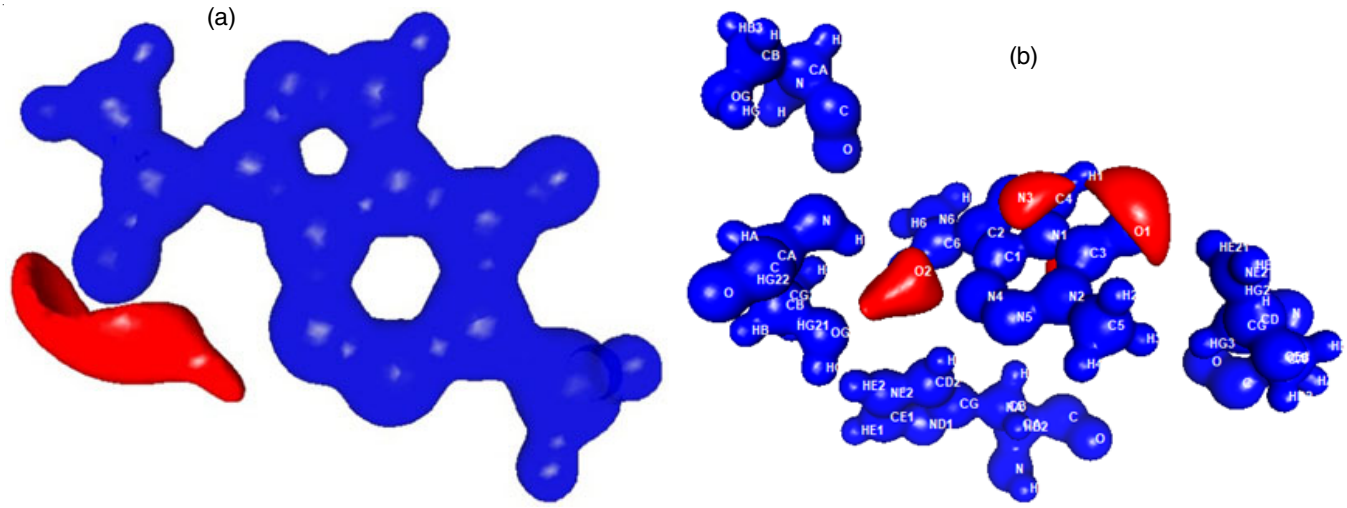

Fig. 5. Isosurface representation of ESP map of TMZ molecule in the (a) gas phase and b) the intermolecular interaction between the TMZ and the active site residues of CA XIII. The positive (blue) surface value is 0.5 eÅ^{-1} and the negative (red) surface value is –0.05 eÅ^{-1}

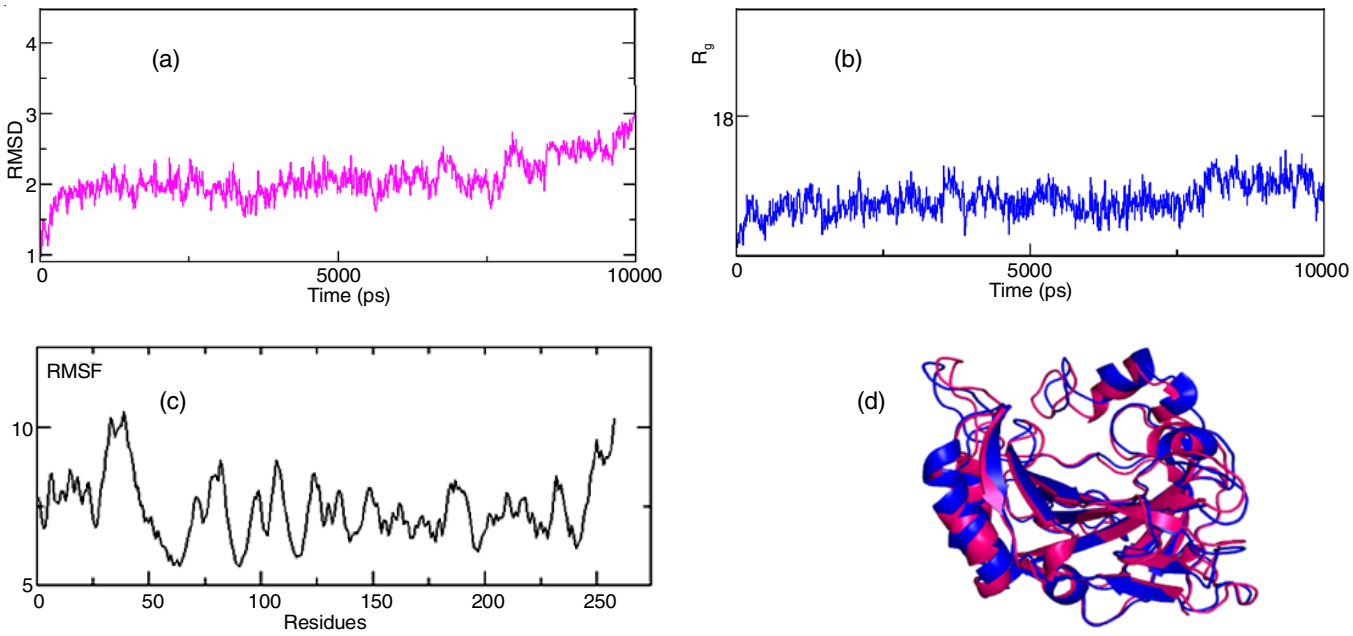

Fig. 6. Trajectories from MD simulation for temo-CA-XIII complex. (a) RMSD; (b) Radius of gyration, (c) RMSF and (d) overlapped view of temo-CA-XIII complex from molecular docking (pink) and MD simulation (blue)

site and isolated phase were studied in detail from QTAIM approach. The corelative topological parameters of temozolomide in the active and gas-phase exhibited the idle effect of the carbonic anhydrase XIII protein on the chemical nature of the ligand. The molecular dynamic simulation study of temozolomide-CA-XIII complex reveals that the conformation and the intermolecular interactions of temozolomide molecule are significantly altered.

REFERENCES

1. A.F. Tamimi and M. Juweid, ed.: S. De Vleeschouwer, Epidemiology and Outcome of Glioblastoma, in: Glioblastoma, Codon Publications, Brisbane, Australia, Chap. 8, pp. 143-153 (2017).
2. E.M. Sizoo, H.R.W. Pasman, L. Dirven, C. Marosi, W. Grisold, R. Grant, G. Stockhammer, J. Egeter, S. Chang, J.J. Heimans, L. Deliens, J.C. Reijneveld and M.J.B. Taphoorn, The End-of-life Phase of High-Grade Glioma Patients: A Systematic Review, *Support. Care Cancer*, **22**, 847 (2014); https://doi.org/10.1007/s00520-013-2088-9
3. D. Wang, C. Wang, L. Wang and Y. Chen, A Comprehensive Review in Improving Delivery of Small-Molecule Chemotherapeutic Agents Overcoming the Blood-Brain/Brain Tumor Barriers for Glioblastoma Treatment, *Drug Deliv.*, **26**, 551 (2019); https://doi.org/10.1080/10717544.2019.1616235
4. H.S. Friedman, T. Kerby and H. Calvert, Temozolomide and Treatment of Malignant Glioma, *Clin. Cancer Res.*, **6**, 2585 (2000).
5. P. Mujumdar, J. Kopecka, S. Bua, C.T. Supuran, C. Riganti and S.A. Poulsen, Carbonic Anhydrase XII Inhibitors Overcome Temozolomide Resistance in Glioblastoma, *J. Med. Chem.*, **62**, 4174 (2019); https://doi.org/10.1021/acs.jmedchem.9b00282
6. M.Y. Mboge, B.P. Mahon, R. McKenna and S.C. Frost, Carbonic Anhydrases: Role in pH Control and Cancer, *Metabolites*, **8**, 19 (2018); https://doi.org/10.3390/metabo8010019
7. A. Zakšauskas, E. Èapkauskaitë, L. Jezepèikas, V. Linkuvienë, M. Kisonaitë, A. Smirnov, E. Manakova, S. Gra•ulis and D. Matulis, Design of Two-Tail Compounds with Rotationally Fixed Benzenesulfonamide Ring as Inhibitors of Carbonic Anhydrases, *Eur. J. Med. Chem.*, **156**, 61 (2018); https://doi.org/10.1016/j.ejmech.2018.06.059
8. Schrödinger, Maestro | Schrödinger, Schrödinger Release 2018-1. (2018).
9. W.L. DeLano, The PyMOL Molecular Graphics System, Version 1.1, Schr{ö}dinger LLC (2002).
10. J.A. Maier, C. Martinez, K. Kasavajhala, L. Wickstrom, K.E. Hauser and C. Simmerling, ff14SB: Improving the Accuracy of Protein Side Chain and Backbone Parameters from ff99SB, *J. Chem. Theory Comput.*, **11**, 3696 (2015); https://doi.org/10.1021/acs.jctc.5b00255
11. D.A. Case, T.E. Cheatham, T. Darden, H. Gohlke, R. Luo, K.M. Merz, A. Onufriev, C. Simmerling, B. Wang and R.J. Woods, The Amber Biomolecular Simulation Programs, *J. Comput. Chem.*, **26**, 1668 (2005); https://doi.org/10.1002/jcc.20290
12. M.F. Harrach and B. Drossel, Structure and Dynamics of TIP3P, TIP4P, and TIP5P Water near Smooth and Atomistic Walls of Different Hydroaffinity, *J. Chem. Phys.*, **140**, 174501 (2014); https://doi.org/10.1063/1.4872239
13. M.P. Jacobson, D.L. Pincus, C.S. Rapp, T.J.F. Day, B. Honig, D.E. Shaw and R.A. Friesner, A Hierarchical Approach to All-Atom Protein Loop Prediction, *Proteins*, **55**, 351 (2004); https://doi.org/10.1002/prot.10613
14. G.J. Martyna, A. Hughes and M.E. Tuckerman, Molecular Dynamics Algorithms for Path Integrals at Constant Pressure, *J. Chem. Phys.*, **110**, 3275 (1999); https://doi.org/10.1063/1.478193
15. D.R. Roe and T.E. Cheatham III, PTRAJ and CPPTRAJ: Software for Processing and Analysis of Molecular Dynamics Trajectory Data, *J. Chem. Theory Comput.*, **9**, 3084 (2013); https://doi.org/10.1021/ct400341p
16. W. Humphrey, A. Dalke and K. Schulten, VMD: Visual Molecular Dynamics, *J. Mol. Graph.*, **14**, 33 (1996); https://doi.org/10.1016/0263-7855(96)00018-5
17. P. Turner, XMGRACE, Version 5.1.19., Cent. Coast. Land-Margin Res. Oregon Grad. Inst. Sci. Technol. Beavert, USA (2005).
18. S. Genheden and U. Ryde, The MM/PBSA and MM/GBSA Methods to Estimate Ligand-Binding Affinities, *Expert Opin. Drug Discov.*, **10**, 449 (2015); https://doi.org/10.1517/17460441.2015.1032936
19. B.R. Miller III, T.D. McGee Jr., J.M. Swails, N. Homeyer, H. Gohlke and A.E. Roitberg, MMPBSA.py: An Efficient Program for End-State Free Energy Calculations, *J. Chem. Theory Comput.*, **8**, 3314 (2012); https://doi.org/10.1021/ct300418h
20. P. Geerlings, F. De Proft and W. Langenaeker, Conceptual Density Functional Theory, *Chem. Rev.*, **103**, 1793 (2003); https://doi.org/10.1021/cr990029p
21. M.J. Frisch, G.W. Trucks, H.B. Schlegel, G.E. Scuseria, M.A. Robb, J.R. Cheeseman, G. Scalmani, V. Barone, B. Mennucci, G.A. Petersson, H. Nakatsuji, M. Caricato, X. Li, H.P. Hratchian, A.F. Izmaylov, J. Bloino, G. Zheng, J.L. Sonnenberg, M. Hada, M. Ehara, K. Toyota, R.

Fukuda, J. Hasegawa, M. Ishida, T. Nakajima, Y. Honda, O. Kitao, H. Nakai, T. Vreven, J.A. Montgomery Jr., J.E. Peralta, F. Ogliaro, M. Bearpark, J.J. Heyd, E. Brothers, K.N. Kudin, V.N. Staroverov, R. Kobayashi, J. Normand, K. Raghavachari, A. Rendell, J.C. Burant, S.S. Iyengar, J. Tomasi, M. Cossi, N. Rega, N.J. Millam, M. Klene, J.E. Knox, J.B. Cross, V. Bakken, C. Adamo, J. Jaramillo, R. Gomperts, R.E. Stratmann, O. Yazyev, A.J. Austin, R. Cammi, C. Pomelli, J.W. Ochterski, R.L. Martin, K. Morokuma, V.G. Zakrzewski, G.A. Voth, P. Salvador, J.J. Dannenberg, S. Dapprich, A.D. Daniels, Ö. Farkas, J.B. Foresman, J.V. Ortiz, J. Cioslowski and D.J. Fox Gaussian 09, Gaussian, Inc., Wallingford CT (2009).

22. AIM2000, *J. Comput. Chem.*, **22**, 545 (2001); https://doi.org/10.1002/1096-987X(20010415)22:5<545::AID-JCC1027>3.0.CO;2-Y
23. C. Köhler, J. Lübben, L. Krause, C. Hoffmann, R. Herbst-Irmer and D. Stalke, Comparison of Different Strategies for Modelling Hydrogen Atoms in Charge Density Analyses, *Acta Crystallogr. B Struct. Sci. Cryst. Eng. Mater.*, **75**, 434 (2019); https://doi.org/10.1107/S2052520619004517
24. A. Stash and V. Tsirelson, WinXPRO: A Program for Calculating Crystal and Molecular Properties Using Multipole Parameters of the Electron Density, *J. Appl. Cryst.*, **35**, 371 (2002); https://doi.org/10.1107/S0021889802003230
25. H. Birkedal, D. Madsen, R.H. Mathiesen, K. Knudsen, H.P. Weber, P. Pattison and D. Schwarzenbach, The Charge Density of Urea from Synchrotron Diffraction Data, *Acta Crystallogr. A*, **60**, 371 (2004); https://doi.org/10.1107/S0108767304015120
26. D.S. Arputharaj, V.R. Hathwar, T.N. Guru Row and P. Kumaradhas, Topological Electron Density Analysis and Electrostatic Properties of Aspirin: An Experimental and Theoretical Study, *Cryst. Growth Des.*, **12**, 4357 (2012); https://doi.org/10.1021/cg300269n
27. A. Volkov, Y. Abramov, P. Coppens and C. Gatti, On the Origin of Topological Differences between Experimental and Theoretical Crystal Charge Densities, *Acta Crystallogr. A*, **56**, 332 (2000); https://doi.org/10.1107/S0108767300003202